Instantaneous Polarimetry With Zak-OTFS

Nishant Mehrotra, Sandesh Rao Mattu, and Robert Calderbank

***Abstract*—Polarimetry, which is the ability to measure the scattering response of the environment across orthogonal polarizations, is fundamental to enhancing wireless communication and radar system performance. In this article, we use the Zak-OTFS modulation to enable *instantaneous* polarimetry within a single transmission frame. We transmit a Zak-OTFS carrier waveform and a spread carrier waveform mutually unbiased to it simultaneously over orthogonal polarizations. The mutual unbiasedness of the two waveforms enables the receiver to estimate the full polarimetric response of the scattering environment from a single received frame. Unlike existing methods for instantaneous polarimetry with computational complexity quadratic in the time–bandwidth product, the proposed method enables instantaneous polarimetry at near-linear complexity in the time–bandwidth product. Via numerical simulations, we show ideal polarimetric target detection and parameter estimation results with the proposed method, with improvements in computational complexity and greater clutter resilience over comparable baselines.**

***Index Terms*—6G, integrated sensing and communication, polarimetry, Zak-OTFS.**

I. Introduction

Polarimetry is an important tool for enhancing the performance of both wireless communication and radar systems. In wireless communication, polarimetry provides a diversity gain [1], [2], [3], [4], thereby improving the reliability of communication, as well as a spatial multiplexing gain [5], [6], [7], [8], which increases the capacity of the wireless link. Similarly, polarimetry increases the waveform degrees of freedom in radar systems [9], [10], [11], [12], [13], [14], [15], [16], [17], [18], providing more information about the target and enabling improved detection of targets with small radar cross section (RCS), such as drones.

Polarimetry is enabled in radar and communication systems by transmitting and receiving on two orthogonal polarizations, e.g., on vertical and horizontal polarizations. The receiver estimates the 2×2 *polarimetric scattering response* of the wireless/radar channel across all four combinations of transmit and receive polarizations. A standard approach is to transmit polarized waveforms *sequentially* across two frames [11], [12], [13], [14], [15]; see Fig. 1(a) for an example with frequency modulated continuous wave (FMCW) transmissions. From its measurements in each frame, the receiver estimates 2×1 slices of the full 2×2 polarimetric scattering response. Such an approach does not provide instantaneous estimates of the scattering response within a single frame. Changes in the scattering environment between the two frames (due to mobility) may partially decorrelate the obtained estimates [12], [13], [14], [15], [16]. Sequential polarimetry also prevents frame-by-frame processing and increases the system latency, which is a critical factor for radar and communication performance in highly dynamic environments. When using continuous waveforms, such as FMCW and pulsed waveforms [19], [20], [21], [22], the computational complexity of sequential polarimetry is *quadratic* in the time–bandwidth product [23], [24], [25].

To unlock the full benefits of polarimetry, it is crucial to estimate the 2×2 polarimetric scattering response *instantaneously* within a single transmission frame. Previous work [13], [14], [15] has proposed transmitting *mutually unbiased* waveforms,[1] i.e., waveforms with small inner products, simultaneously across orthogonal polarizations. Mutual unbiasedness ensures that the contribution of the other waveform looks like noise to the receiver when it projects its measurements onto the basis of one of the transmit waveforms. Projecting its measurements onto the basis of each of the two transmit waveforms provides the receiver with an estimate of different 2×1 slices of the polarimetric scattering response, thus enabling full 2×2 polarimetric scattering response estimation from a single received frame. Mutually unbiased waveforms have been designed in prior work [13], [14], [15] via *phase-coding*, i.e., by modulating a common carrier waveform, e.g., a rectangular waveform, with mutually unbiased sequences, e.g., Zadoff–Chu sequences with distinct roots [13] or complementary Golay pairs [14], [15]. While this approach offers excellent polarimetric target detection and parameter estimation (detailed later in Section IV), the computational complexity of polarimetry via phase-coding remains *quadratic* in the time–bandwidth product [25], [27]. Moreover, we have shown in [25] that separate selection of sequences and carrier waveforms, as done in phase-coding, may be suboptimal from a radar waveform design perspective.

In this article, we take an alternate approach to constructing mutually unbiased waveforms for instantaneous polarimetry using the *Zak-OTFS* (orthogonal time–frequency space) modulation [28], [29], [30] in place of phase-coding. The carrier waveform in Zak-OTFS, termed *pulsone*, is a pulse localized in the delay–Doppler (DD) domain. We use a generalized discrete affine Fourier transform [25], [31] to transform the pulsone into a spread waveform that is mutually unbiased to the pulsone. Our approach has two advantages over phase-coding. First, scattering response estimation with pulsones and their unitary transformations is possible with colorblacknear-linear computational complexity in the time–bandwidth product [25]. Second, unlike phase-coding, Zak-OTFS enables *joint optimization* of sequences and carrier waveforms, which has been shown to be optimal from a radar waveform design perspective in [25]. We illustrate our proposed approach in Fig. 1(b) and describe it in more detail in Section III.

Table I places our contributions in the context of prior work, which is described in more detail in Section II. In addition to the advantages in computational complexity and latency, our proposed approach also improves upon the number of simultaneously detectable targets and the Doppler resolution over the sequential approach based on FMCW. Moreover, in Section IV we demonstrate that the proposed approach achieves ideal polarimetric target detection and parameter

Received 26 August 2025; revised 21 October 2025; accepted 23 October 2025. Date of publication 27 October 2025; date of current version 6 November 2025. This work was supported in part by the National Science Foundation under Grant 2342690 and Grant 2148212, in part by the Funds From Federal Agency and Industry Partners as Specified in the Resilient and Intelligent NextG Systems (RINGSs) Program, and in part by the Air Force Office of Scientific Research under Grant FA 8750-20-2-0504 and Grant FA 9550-23-1-0249. *(Nishant Mehrotra and Sandesh Rao Mattu contributed equally to this work.) (Corresponding author: Nishant Mehrotra.)*

The authors are with the Department of Electrical and Computer Engineering, Duke University, Durham, NC 27708 USA (e-mail: nishant.mehrotra@duke.edu; sandesh.mattu@duke.edu; robert.calderbank@duke.edu).

Digital Object Identifier 10.1109/TRS.2025.3625812

[1]The term "mutually unbiased" is from quantum information theory [26]. Formally, two d-length waveforms are mutually unbiased if their inner product has magnitude $1/\sqrt{d}$. Measurements from one waveform are "statistically independent" to those from the other waveform with uniform probability $1/d$.

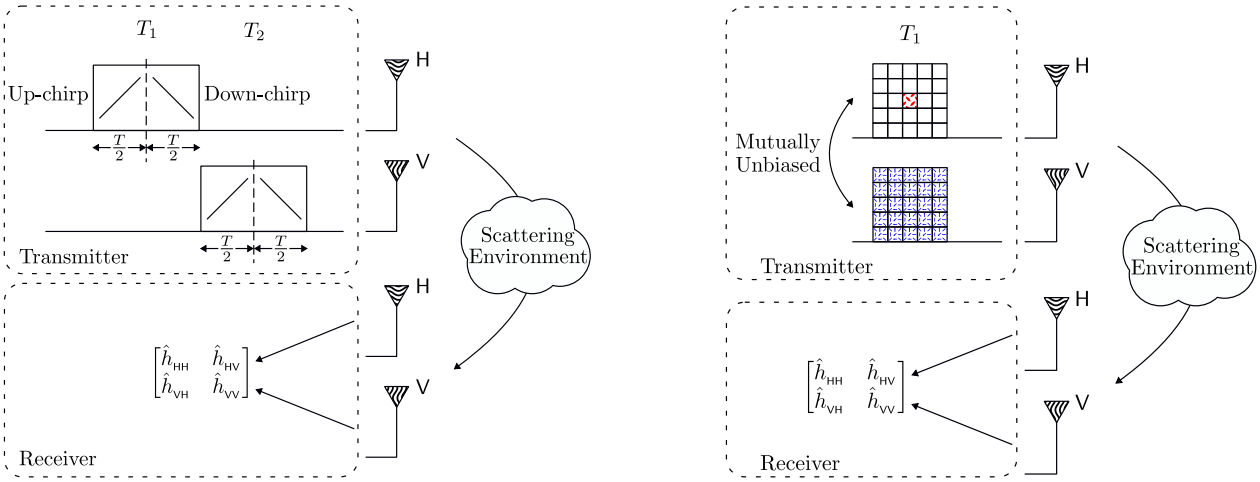

(a) Sequential Polarimetry with FMCW

(b) Instantaneous Polarimetry with Zak-OTFS (Ours)

Fig. 1. Comparison of different approaches for polarimetry. (a) Sequential polarimetry with FMCW transmits polarized FMCW waveforms over two frames, with each frame subdivided into two halves with an up-chirp and a down-chirp, respectively. The associated Doppler resolution is $2/T$ and the computational complexity is $\mathcal{O}(B^2T^2)$. (b) Instantaneous polarimetry with Zak-OTFS transmits a Zak-OTFS pulsone and a mutually unbiased spread waveform obtained via a unitary transformation of the pulsone in a single frame. Compared with the sequential approach in (a), the proposed approach has $2\times$ smaller latency, $2\times$ improved Doppler resolution of $1/T$, and a computational complexity of only $\mathcal{O}(BT\log T)$.

TABLE I

COMPARISON OF DIFFERENT APPROACHES FOR POLARIMETRY; B DENOTES SIGNALING BANDWIDTH AND T DENOTES FRAME INTERVAL

Approach	Frame(s)	Target(s)	Doppler Res.	Complexity
Zak-OTFS (Ours)	1	> 1	$1/T$	$O(BT \log T)$
Phase-coded [13]–[15]	1	> 1	$1/T$	$O(B^2T^2)$
FMCW [12], [19]	2	1	$2/T$	$O(B^2T^2)$

estimation[2] and greater clutter resilience compared with the phase-coded approach at smaller computational complexity.

Notation: x denotes a complex scalar, $\mathbf{x}$ denotes a vector with the nth entry $\mathbf{x}[n]$, and $\mathbf{X}$ denotes a matrix with the (n,m)th entry $\mathbf{X}[n,m]$. $(\cdot)^*$ denotes complex conjugate, $(\cdot)^\top$ denotes transpose, $(\cdot)^H$ denotes complex conjugate transpose, and $\langle \mathbf{x}, \mathbf{y}\rangle = \sum_n \mathbf{x}[n]\mathbf{y}^*[n]$ denotes the inner product. Calligraphic font $\mathcal{X}$ denotes operators or sets, with usage clear from context. $\emptyset$ denotes the empty set. $\mathbb{Z}$ denotes the set of integers and $\mathbb{Z}_N$ the set of integers modulo N. (a,b) denotes the greatest common divisor of two integers a, b. $(\cdot)_N$ denotes the value modulo N and $(\cdot)_N^{-1}$ denotes the inverse modulo N. $\delta(\cdot)$ denotes the delta function, $\delta[\cdot]$ denotes the Kronecker delta function, and $\mathbf{I}_N$ denotes the $N \times N$ identity matrix.

II. POLARIMETRY: PRELIMINARIES

As described in the Introduction, polarimetry is enabled in radar and communication systems by transmitting and receiving on orthogonal polarizations, e.g., on vertical and horizontal polarizations, using dual-polarized antennas. Let V and H, respectively, denote vertical and horizontal polarizations. We now describe how to model the polarimetric scattering response of a P-path wireless/radar channel. In unipolarized systems, the channel gain of each path $p \in \{1, \ldots, P\}$ is modeled by a complex scalar $h^{(p)}$. With dual-polarized transmit and receive antennas, the channel gain is modeled instead by a 2×2 *polarimetric scattering response* [10], [11], [12], [13], [14], [15]

$$\boldsymbol{H}^{(p)} = \begin{bmatrix} h_{HH}^{(p)} & h_{HV}^{(p)} \\ h_{VH}^{(p)} & h_{VV}^{(p)} \end{bmatrix} = \mathbf{C}_{\mathsf{RX}} \boldsymbol{\Sigma}^{(p)} \mathbf{C}_{\mathsf{TX}} \tag{1}$$

where $\mathbf{C}_{\mathsf{TX}}$ (resp. $\mathbf{C}_{\mathsf{RX}}$) is a 2×2 matrix characterizing the polarization coupling at the transmitter (resp. receiver), and $\boldsymbol{\Sigma}^{(p)}$ is a 2×2 matrix of polarimetric scattering coefficients of the pth path/target.[3] Broadly stated, the goal in polarimetry is to estimate all the four components of the polarimetric scattering response in (1) from the measurements at the receiver. We now describe two approaches for polarimetry from previous work, before outlining our proposed approach in Section III.

A. Sequential Polarimetry via FMCW

As described in the Introduction, a standard approach for enabling polarimetry is to transmit polarized waveforms sequentially across two frames. Fig. 1(a) illustrates sequential polarimetry using FMCW waveforms [12], [19], [20], [21], [22] (chirps), although the underlying approach is applicable to any waveform. In frame interval T_1 (resp. T_2), the same waveform is transmitted in horizontal (resp. vertical) polarization. From its measurements in frame interval T_1 (resp. T_2), the receiver obtains maximum likelihood estimates for $h_{HH}^{(p)}$ and $h_{VH}^{(p)}$ (resp. $h_{VH}^{(p)}$ and $h_{VV}^{(p)}$) by cross-correlating its dual-polarized received signals and the transmitted waveform [12], [19], [20], [21], [22].

In the specific case of sequential polarimetry via FMCW, it is known from [23], [24], [25] that cross-correlation-based channel estimation has computational complexity $\mathcal{O}(B^2T^2)$, quadratic in the time–bandwidth product BT. Localizing a single path/target with FMCW requires *subdividing* each frame interval T_1 or T_2 into two halves and transmitting a chirp with positive slope ("up-chirp") and a chirp with negative slope ("down-chirp") in each half [23], [24], yielding an effective Doppler resolution of $2/T$. Localizing multiple paths/targets with this approach[4] results in multiple false ("ghost") targets [23], [24], degrading the detection performance. Moreover,

[2]The results in this article serve as a proof-of-concept numerical demonstration of the concept; hardware demonstration will be pursued in future work. Potential challenges include managing the peak-to-average power ratio (PAPR) and over-the-air synchronization. With regards to the former, we note that a natural advantage of the proposed framework is its low PAPR of only 5.6 dB; see [25, Section IV.2] and [31] for details. This reduction in PAPR has also been experimentally demonstrated in [32] in the subterahertz band.

[3]$\boldsymbol{\Sigma}^{(p)} = \mathbf{I}_2$ for a line-of-sight path with no reflection.

[4]It is possible to localize multiple paths/targets by subdividing each frame into four quarters with further degraded Doppler resolution of $4/T$ [23], [24].

the high sidelobes of FMCW make detecting weak targets in the presence of stronger ones challenging [24], [25].

There are two primary drawbacks of the sequential approach independent of the drawbacks due to the choice of waveform. First, it requires the scattering environment to remain constant across two frames. Second, it prevents frame-by-frame processing. We now describe an approach for instantaneous polarimetry that overcomes these two drawbacks.

B. Instantaneous Polarimetry via Phase-Coding

Instantaneous polarimetry overcomes the two drawbacks of sequential polarimetry by transmitting *mutually unbiased* waveforms simultaneously across both the polarizations. Fig. 1(b) illustrates the main idea. In a single frame interval, unit-norm waveforms $\mathbf{x}_V(t)$ and $\mathbf{x}_H(t)$ satisfying the property $\left|\int \mathbf{x}_H(t)\mathbf{x}_V^*(t-\tau)e^{-j2\pi\nu(t-\tau)}\mathrm{dt}\right| \ll 1$ are transmitted in vertical and horizontal polarizations. The receiver estimates all four components of the 2×2 matrix $\boldsymbol{H}^{(p)}$ from (1) by cross-correlating its dual-polarized received signals with the corresponding transmitted waveform. For example, the receiver estimates $h_{VH}^{(p)}$ by cross-correlating its received signal in vertical polarization with $\mathbf{x}_H(t)$.

Mutually unbiased waveforms have been designed in previous work [13], [14], [15] by phase coding a common carrier waveform with mutually unbiased discrete sequences, e.g., Zadoff–Chu sequences with distinct roots. The primary drawback of phase-coding is that the computational complexity of cross correlation remains quadratic in the time–bandwidth product, $\mathcal{O}(B^2T^2)$ [25], [27]. In Section III, we describe how to design mutually unbiased waveforms using the Zak-OTFS modulation to enable instantaneous polarimetry with only $\mathcal{O}(BT\log T)$ computational complexity.

III. Instantaneous Polarimetry via Zak-OTFS

We provide a brief overview of Zak-OTFS in the standard unipolarized setting in Section III-A, referring the interested reader to [28], [29], and [30] for a more detailed description of Zak-OTFS. We then extend the system model to polarimetry in Section III-B and detail our proposed approach in Section III-C.

A. Overview of Zak-OTFS

The Zak-OTFS carrier waveform is a pulse in the DD domain, formally a quasi-periodic localized function termed the *DD pulsone*.[5] The DD pulsone is characterized by a delay period τ_p and a Doppler period ν_p, with $\tau_p\nu_p = 1$. The DD pulsone occupies infinite time and bandwidth. For practical implementation, the DD pulsone is limited to a time interval T and a bandwidth B via DD domain pulse shaping. The DD pulsone defines an orthonormal basis within the delay and Doppler periods with $BT = MN$ basis elements at $M = \tau_p/1_B = B\tau_p$ distinct locations along delay and $N = \nu_p/1_T = T\nu_p$ distinct locations along Doppler.

The DD pulsone is converted into a TD waveform via the inverse Zak transform [28], [29], [30]. After Nyquist sampling, the discrete TD pulsone waveform is [28], [29], [30]

$$\mathbf{p}_{(k_0,l_0)}[n] = \frac{1}{\sqrt{N}}\sum_{d\in\mathbb{Z}} e^{\frac{j2\pi}{N}dl_0}\delta[n-k_0-\mathrm{dM}] \tag{2}$$

where $k_0 \in \mathbb{Z}_M$ indexes the location of the pulsone as a multiple of the delay resolution $1_B = \tau_p/M$, and $l_0 \in \mathbb{Z}_N$ indexes the location of the pulsone as a multiple of the Doppler resolution $1_T = \nu_p/N$. The discrete TD signal on mounting MN information symbols on the TD pulsones in (2) is

$$\mathbf{x}[n] = \sum_{k_0=0}^{M-1}\sum_{l_0=0}^{N-1}\mathbf{X}[k_0,l_0]\,\mathbf{p}_{(k_0,l_0)}[n] \tag{3}$$

where $\mathbf{X}$ denotes the $M\times N$ array of information symbols.

[5]Termed "pulsone" due to its structure of a pulse train modulated by a tone in the time domain (TD), see [29, Fig. 2] for an illustration.

After pulse shaping, the transmitted signal interacts with the scattering environment and is matched filtered at the receiver. The discrete TD received signal is given by [25], [28], and [31]

$$\mathbf{y}[n] = \sum_{k,l\in\mathbb{Z}_{MN}} \mathbf{h}_{\mathrm{eff}}[k,l]\,\mathbf{x}\left[(n-k)_{MN}\right]e^{\frac{j2\pi}{\mathrm{MN}}l(n-k)} + \mathbf{w}[n] \tag{4}$$

where $\mathbf{h}_{\mathrm{eff}}[k,l]$ denotes the *effective channel*[6] that encompasses the effects of the physical scattering environment and transmit and receive pulse shaping/matched filtering [30, Eq. (7)], and $\mathbf{w}[n]$ denotes the additive noise at the receiver. For a scattering environment with P paths/targets, let $\mathbf{h}_{\mathrm{phy}}(\tau,\nu) = \sum_{t=1}^{P} h^{(p)}\delta(\tau-\tau_t)\delta(\nu-\nu_t)$ denote the corresponding channel representation in the continuous DD domain. The effective channel is given by samples of the continuous effective channel, $\mathbf{h}_{\mathrm{eff}}[k,l] = \mathbf{h}_{\mathrm{eff}}(\tau=(k\tau_p)/M, \nu=(l\nu_p)/N)$, where [28], [29], [30]

$$\mathbf{h}_{\mathrm{eff}}(\tau,\nu) = \mathbf{w}_{\mathrm{RX}}(\tau,\nu) *_\sigma \mathbf{h}_{\mathrm{phy}}(\tau,\nu) *_\sigma \mathbf{w}_{\mathrm{TX}}(\tau,\nu). \tag{5}$$

In (5), $\mathbf{w}_{\mathrm{TX}}(\tau,\nu)$ denotes the transmit pulse shaping filter, e.g., $\mathbf{w}_{\mathrm{TX}}(\tau,\nu) = (BT)^{1/2}\,\mathrm{sinc}(B\tau)\,\mathrm{sinc}(T\nu)$ for sinc pulse shaping [33], $\mathbf{w}_{\mathrm{RX}}(\tau,\nu) = e^{j2\pi\nu\tau}\mathbf{w}_{\mathrm{TX}}^*(-\tau,-\nu)$ denotes the receiver matched filter, and $*_\sigma$ denotes twisted convolution.[7]

The effective channel is estimated at the receiver via the *cross-ambiguity function*[8] [24], [25], [31], [33]

$$\begin{aligned}\widehat{\mathbf{h}}_{\mathrm{eff}}[k,l] &= \mathbf{A}_{\mathbf{y},\mathbf{x}}[k,l]\\ &= \sum_{n=0}^{\mathrm{MN}-1}\mathbf{y}[n]\,\mathbf{x}^*\left[(n-k)_{MN}\right]e^{-\frac{j2\pi}{\mathrm{MN}}l(n-k)}\end{aligned} \tag{6}$$

whose peaks in the absolute value indicate delay and Doppler bins of potential targets in the scattering environment. It has been shown in [24] and [25] that computing the cross-ambiguity function in Zak-OTFS requires only $\mathcal{O}(BT\log T)$ complexity.

Accurate channel estimation is possible when the sequence $\mathbf{x}$ satisfies the *crystallization condition* [28], [29], [30], [31], [33]. Let $\mathcal{S} = \{(k,l)\,|\,|\mathbf{A}_{\mathbf{x},\mathbf{x}}[k,l]| = 1\}$ denote the DD locations where the self-ambiguity function of $\mathbf{x}$ is unimodular, and let $\mathcal{C}$ denote the maximum DD support of the scattering environment.[9] The crystallization condition requires

$$\left(\bigcup_{(k,l)\in\mathcal{S}}(\mathcal{C}+(k,l))\right)\cap\left(\bigcup_{(k',l')\in\mathcal{S}}(\mathcal{C}+(k',l'))\right)=\emptyset \tag{7}$$

where $(k,l)\neq(k',l')$. In other words, translates of the channel support by locations where the self-ambiguity function is unimodular must not overlap for accurate channel estimation.

B. Extension to Polarimetry

The system model in (4) is extended to polarimetry as

$$\begin{aligned}\mathbf{y}^{(j)}[n] = &\sum_{i\in\{V,H\}k,l\in\mathbb{Z}_{MN}}\mathbf{h}_{\mathrm{eff}}^{(j,i)}[k,l]\,\mathbf{x}^{(i)}\left[(n-k)_{MN}\right]e^{\frac{j2\pi}{\mathrm{MN}}l(n-k)}\\ &+\mathbf{w}^{(j)}[n],\quad i,j\in\{V,H\}\end{aligned} \tag{8}$$

where $\mathbf{x}^{(i)}$ denotes the signal transmitted by the i-polarized transmit antenna, $\mathbf{h}_{\mathrm{eff}}^{(j,i)}[k,l]$ denotes the effective channel between the i-polarized transmit antenna and the j-polarized receive antenna, and $\mathbf{w}^{(j)}[n]$ denotes the additive noise at the j-polarized receive antenna. In (8), the polarimetric effective channel $\mathbf{h}_{\mathrm{eff}}^{(j,i)}[k,l]$ is defined similar to (5) using the polarimetric continuous DD channel representation, $\mathbf{h}_{\mathrm{phy}}^{(j,i)}(\tau,\nu) = \sum_{t=1}^{P} h_{\mathrm{ji}}^{(p)}\delta(\tau-\tau_t)\delta(\nu-\nu_t)$, where $h_{\mathrm{ji}}^{(p)}$ is the (j,i)th entry of the matrix $\boldsymbol{H}^{(p)}$ in (1).

[6]The effective channel approximates the physical channel when all the paths are resolvable in delay with bandwidth B and in Doppler with time T.

[7]$a(\tau,\nu)*_\sigma b(\tau,\nu) = \int a(\tau',\nu')b(\tau-\tau',\nu-\nu')e^{j2\pi\nu'(\tau-\tau')}d\tau'd\nu'$.

[8]When $\mathbf{y}=\mathbf{x}$, the expression $\mathbf{A}_{\mathbf{x},\mathbf{x}}[k,l]$ is called the self-ambiguity.

[9]e.g., $\mathcal{C} = [k_{\min},k_{\max}]\times[l_{\min},l_{\max}]$ based on prior knowledge of the minimum/maximum delay and Doppler spreads of the scattering environment.

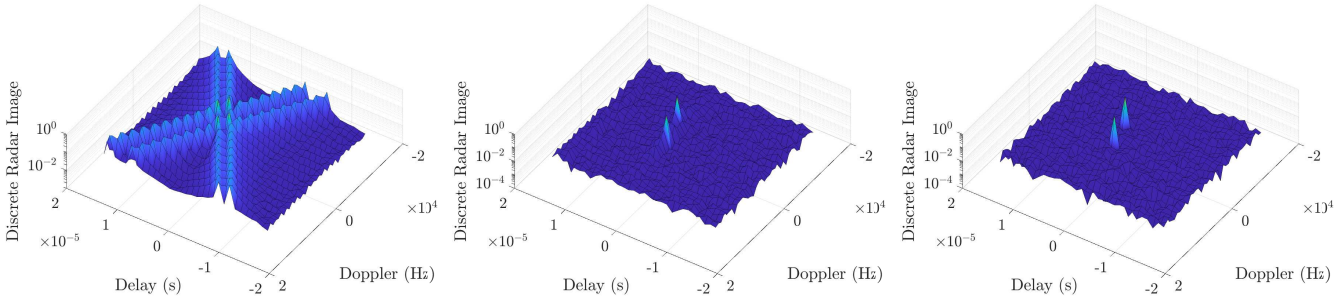

(a) FMCW, HH (b) Phase-coded, HH (c) Zak-OTFS, HH

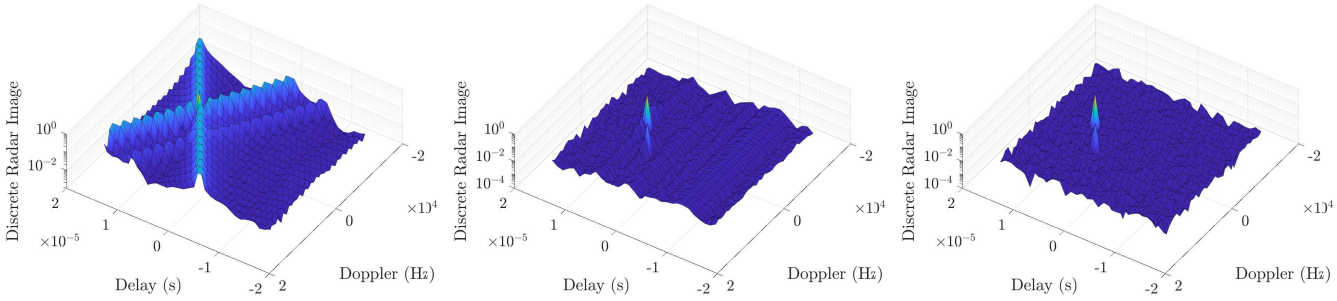

(d) FMCW, VH (e) Phase-coded, VH (f) Zak-OTFS, VH

Fig. 2. Heatmaps of estimated channels for a four-target environment with two targets with equal $h_{HH}^{(p)} = 0.7$ & $h_{HV}^{(p)} = h_{VH}^{(p)} = h_{VV}^{(p)} = 0$, and two targets with unequal $h_{HV}^{(p)} = h_{VH}^{(p)} \in \{0.3, 0.95\}$ & $h_{HH}^{(p)} = h_{VV}^{(p)} = 0$. (a) and (d) Sequential polarimetry via FMCW detects two false targets ("ghost targets") in addition to the two true targets in the HH channel and fails to detect the lower energy target in the VH channel due to the high sidelobes of the waveform. (b) and (c) and (e) and (f) Instantaneous polarimetry via mutually unbiased phase-coded and Zak-OTFS waveforms detects all four targets correctly in the HH and VH channels.

C. Proposed Approach for Instantaneous Polarimetry

We enable instantaneous polarimetry at near-linear complexity by designing mutually unbiased sequences via Zak-OTFS. To that end, in the following we define the generalized discrete affine Fourier transform (GDAFT) [25], [31], which maps pulsones in (2) to mutually unbiased spread waveforms. We have used the GDAFT to design radar waveform libraries in [25] and for spread carrier communication in [31].

Definition 1 ([25], [31]): The generalized discrete affine Fourier transform (GDAFT) of an MN-length sequence $\mathbf{x}$ is

$$\mathcal{F}_a \mathbf{x}[n] = \frac{1}{\sqrt{MN}} \sum_{m=0}^{\mathrm{MN}-1} e^{\frac{j2\pi}{\mathrm{MN}}\left(An^2+Bnm+Cm^2\right)} \mathbf{x}[m]$$

where $n \in \{0, \ldots, MN-1\}$, A, B, C are coprime to MN.

Theorem 1 ([25], [31]): The GDAFT in Definition 1 maps the discrete time pulsone in (2) localized at (k_0, l_0) in the discrete DD domain to the spread carrier sequence

$$\mathbf{c}[n] = \mathcal{F}_a \mathbf{p}_{(k_0,l_0)}[n] = \frac{e^{\frac{j2\pi}{\mathrm{MN}}\left(An^2+Bnk_0+Ck_0^2\right)}}{\sqrt{MN}} \epsilon_N \left(\frac{\mathrm{CM}}{N}\right)_J \times e^{-\frac{j2\pi}{N}(4\mathrm{CM})_N^{-1}\left(\mathrm{Bn}+l_0+2Ck_0\right)^2}$$

where $\epsilon_N = 1$ if $N \equiv 1 \bmod 4$ & $\epsilon_N = j$ if $N \equiv 3 \bmod 4$, and $(a/b)_J$ denotes the Jacobi symbol.

A useful consequence of Theorem 1 is that the output of the GDAFT is mutually unbiased to the pulsone [25], [31]

$$\mathbf{A}_{\mathbf{c},\mathbf{p}_{(k_0,l_0)}}[k,l] = \frac{C_{(k_0,l_0)}[k,l]}{\sqrt{MN}} \tag{9}$$

where $C_{(k_0,l_0)}[k,l]$ is a complex phase, $\left|C_{(k_0,l_0)}[k,l]\right| = 1$, and $\mathbf{A}_{\mathbf{y},\mathbf{x}}[k,l]$ denotes the cross-ambiguity function as in (6). Moreover, the GDAFT *preserves* the near-linear computational complexity of cross-ambiguity-based channel estimation [25].

For instantaneous polarimetry, we transmit the pulsone and the output of the GDAFT in orthogonal polarizations, e.g.,

$$\mathbf{x}^{(H)}[n] = \mathbf{p}_{(k_0,l_0)}[n], \quad \mathbf{x}^{(V)}[n] = \mathbf{c}[n]. \tag{10}$$

For accurate channel estimation, the GDAFT parameters A, B, C in Theorem 1 are chosen such that $\mathbf{c}[n]$ satisfies the crystallization condition in (7) for all four components of the polarimetric effective channel $\mathbf{h}_{\mathrm{eff}}^{(j,i)}[k,l]$, for all $i, j \in \{V, H\}$. For a detailed discussion on GDAFT parameter selection, see Fig. 1 and the associated example in [31, Section IV-C].

On obtaining the received signals per (8), the receiver computes the cross-ambiguity function per (6) between $\mathbf{y}^{(j)}$ and $\mathbf{x}^{(i)}$ to estimate the effective channel $\mathbf{h}_{\mathrm{eff}}^{(j,i)}[k,l]$, for all $i, j \in \{V, H\}$. We now show how mutual unbiasedness per (9) enables accurate estimation of all four polarimetric effective channels $\mathbf{h}_{\mathrm{eff}}^{(j,i)}[k,l]$. Without loss of generality, we prove the result for the example considered in (10).

The estimate of $\mathbf{h}_{\mathrm{eff}}^{(j,i)}[k,l]$ from (6) and (8) is given by

$$\begin{aligned}
\widehat{\mathbf{h}}_{\mathrm{eff}}^{(j,i)}[k,l] &= \mathbf{A}_{\mathbf{y}^{(j)},\mathbf{x}^{(i)}}[k,l] \\
&= \sum_{n=0}^{\mathrm{MN}-1} \mathbf{y}^{(j)}[n] \left(\mathbf{x}^{(i)}\right)^* \left[(n-k)_{MN}\right] e^{-\frac{j2\pi}{\mathrm{MN}} l(n-k)} \\
&= \sum_{i' \in \{V,H\}} \sum_{k',l'} \mathbf{h}_{\mathrm{eff}}^{(j,i')}[k',l'] \sum_{n=0}^{\mathrm{MN}-1} \mathbf{x}^{(i')}\left[(n-k')_{MN}\right] \\
&\quad \times e^{\frac{j2\pi}{\mathrm{MN}} l'(n-k')} \left(\mathbf{x}^{(i)}\right)^* \left[(n-k)_{MN}\right] e^{-\frac{j2\pi}{\mathrm{MN}} l(n-k)} \\
&\quad + \mathbf{A}_{\mathbf{w}^{(j)},\mathbf{x}^{(i)}}[k,l].
\end{aligned} \tag{11}$$

For additive noise $\mathbf{w}^{(j)}$ uncorrelated with the transmitted signals $\mathbf{x}^{(i)}$, we have $\mathbf{A}_{\mathbf{w}^{(j)},\mathbf{x}^{(i)}}[k,l] = 0$, for all k, l. On further making the substitution $n' = (n-k')_{MN}$ we obtain

$$\widehat{\mathbf{h}}_{\mathrm{eff}}^{(j,i)}[k,l] = \sum_{i' \in \{V,H\}} \sum_{k',l'} \mathbf{h}_{\mathrm{eff}}^{(j,i')}[k',l'] \sum_{n'=0}^{\mathrm{MN}-1} \mathbf{x}^{(i')}[n'] e^{\frac{j2\pi}{\mathrm{MN}} l'n'}$$

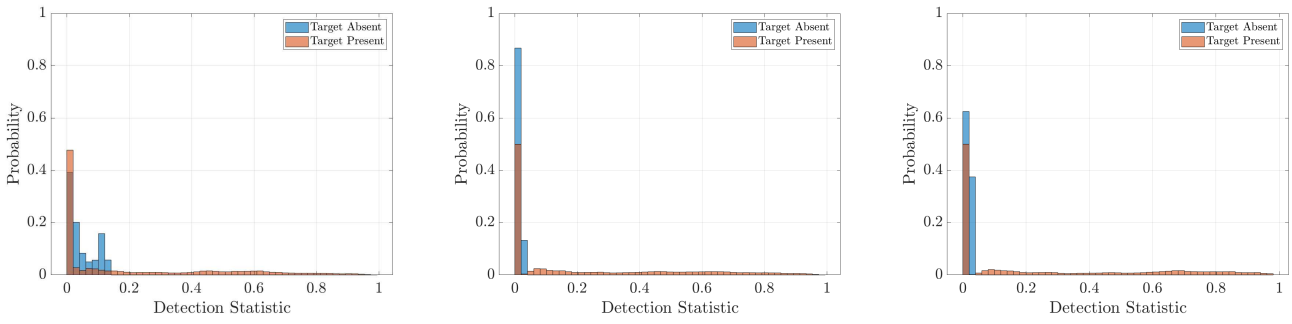

(a) FMCW, uni-polarized (b) Phase-coded, uni-polarized (c) Zak-OTFS, uni-polarized

(d) FMCW, dual-polarized (e) Phase-coded, dual-polarized (f) Zak-OTFS, dual-polarized

Fig. 3. Histograms for single polarimetric target detection under the target present and target absent hypotheses. (a)–(c) Unipolarization is insufficient for detecting polarimetric targets. (d) Dual-polarized FMCW is not optimal for polarimetric target detection due to high waveform sidelobes & false target detections [cf. Fig. 2(a) and (d)]. (e) and (f) Dual-polarized phase-coded and Zak-OTFS waveforms are optimal for polarimetric target detection [cf. Fig. 2(b) and (c) and 2(e) and (f)].

$$\begin{aligned}
&\times \left(\mathbf{x}^{(i)}\right)^{*}\left[\left(n'-(k-k')_{MN}\right)_{MN}\right] e^{-\frac{j2\pi}{MN}l\left(n'-(k-k')\right)} \\
&= \sum_{i'\in\{V,H\}}\sum_{k',l'} \mathbf{h}_{\text{eff}}^{(j,i')}\left[k',l'\right] e^{\frac{j2\pi}{MN}l'(k-k')} \\
&\quad \times \mathbf{A}_{\mathbf{x}^{(i')},\mathbf{x}^{(i)}}\left[(k-k')_{MN},(l-l')_{MN}\right] \\
&= \sum_{i'\in\{V,H\}} \mathbf{h}_{\text{eff}}^{(j,i')}[k,l] *_{\sigma} \mathbf{A}_{\mathbf{x}^{(i')},\mathbf{x}^{(i)}}[k,l] \qquad (12)
\end{aligned}$$

where $*_{\sigma}$ denotes discrete twisted convolution [28], [29], [30], [33].

The expression in (12) is the sum of two terms

$$\begin{aligned}
\widehat{\mathbf{h}}_{\text{eff}}^{(j,i)}[k,l] &= \mathbf{h}_{\text{eff}}^{(j,i)}[k,l] *_{\sigma} \mathbf{A}_{\mathbf{x}^{(i)},\mathbf{x}^{(i)}}[k,l] \\
&\quad + \mathbf{h}_{\text{eff}}^{(j,\bar{i})}[k,l] *_{\sigma} \mathbf{A}_{\mathbf{x}^{(\bar{i})},\mathbf{x}^{(i)}}[k,l] \qquad (13)
\end{aligned}$$

where $\bar{i}$ denotes a polarization different from i in the set $\{V,H\}$. Since each sequence $\mathbf{x}^{(i)}$ satisfies the crystallization condition in (7), the first term is simply $\mathbf{h}_{\text{eff}}^{(j,i)}[k,l]$. To simplify the second term, we substitute (9) to obtain

$$\begin{aligned}
\widehat{\mathbf{h}}_{\text{eff}}^{(j,i)}[k,l] &= \mathbf{h}_{\text{eff}}^{(j,i)}[k,l] + \mathbf{h}_{\text{eff}}^{(j,\bar{i})}[k,l] *_{\sigma} \frac{C[k,l]}{\sqrt{MN}} \\
&\approx \mathbf{h}_{\text{eff}}^{(j,i)}[k,l] \qquad (14)
\end{aligned}$$

where $C[k,l]$ is a phase term similar to that in (9). Since the second term is the twisted convolution of the effective channel $\mathbf{h}_{\text{eff}}^{(j,\bar{i})}[k,l]$ with a constant amplitude term, it simply raises the noise floor of the channel estimate. Computing each cross-ambiguity term only incurs $\mathcal{O}(BT\log T)$ complexity,[10] and the overall complexity remains near-linear in BT.

[10]The complexity reduction from quadratic to near-linear is due to the symmetry of the Zak-OTFS carrier waveform. Specifically, the cross-ambiguity function computation with Zak-OTFS carrier waveforms reduces to an fast Fourier transform (FFT) calculation. For more details, see [25].

IV. Numerical Results

We now qualitatively and quantitatively compare the performance of the proposed approach from Section III with sequential polarimetry via FMCW (Section II-A) and instantaneous polarimetry via phase-coding (Section II-B). We also compare against unipolarized systems. Our initial results are limited to target detection and estimation in the presence of noise; extensions to clutter are briefly pursued in Section IV-C.

We simulate a monostatic polarimetric radar with frame transmissions of bandwidth $B = 930$ kHz and time $T = 1.2$ ms. For FMCW transmissions, in each frame we simulate up-chirps and down-chirps occupying bandwidth B and time $T/2$ each as described in Section II-A sampled at $f_s = 2B$. For phase-coded transmissions, we consider a rectangular carrier waveform with BT chips of length $1/B$ sampled at $f_s = 2B$, which is modulated by Zadoff–Chu sequences of roots $u \in \{101, 107\}$. For Zak-OTFS, we consider a delay period of $\tau_p = 33.33$ μs and a Doppler period of $\nu_p = 30$ kHz, which correspond to $M = 31$ and $N = 37$ resolvable locations along delay and Doppler, respectively. We assume sinc pulse shaping [33]. Unless noted otherwise, we add white Gaussian noise $\mathbf{w}^{(j)}$ to the received signals in (8).

A. Polarimetric Channel Estimation (Qualitative)

Fig. 2 qualitatively shows comparison of the performance of polarimetric channel estimation via the cross-ambiguity function[11] in (6) for a four-target scattering environment. We simulate two targets

[11]For our implementation on a CPU cluster with 36 cores and 64-GB memory, the median time for cross-ambiguity computation with frame size $M = 31$, $N = 37$ is 2.4363 s for FMCW with median absolute deviation 0.081 s, 2.3445 s for phase-coded with median absolute deviation 0.0868 s, and 0.0012 s for Zak-OTFS with median absolute deviation 45.044 μs, consistent with the computational complexity analysis in Section III.

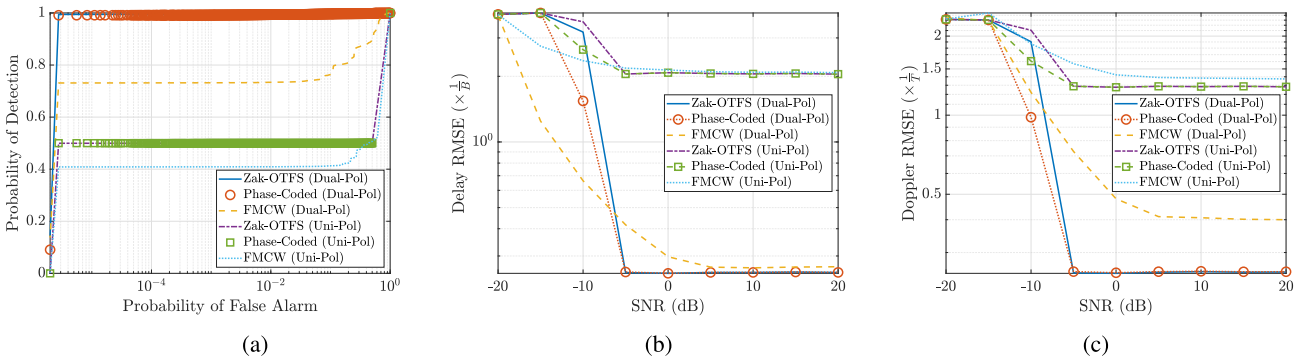

Fig. 4. Single target detection and estimation performance. (a) ROC curve showing ideal target detection with dual-polarized Zak-OTFS and phase-coded waveforms. The performance degrades with FMCW and/or unipolarized waveforms. (b) and (c) RMSE for delay and Doppler estimation, normalized by the corresponding delay and Doppler resolutions of $1/B$ and $1/T$. (b) Delay RMSE is similar for dual-polarized Zak-OTFS, phase-coded and FMCW systems at high SNR, with significant improvements over unipolarized waveforms. (c) Doppler RMSE is similar for dual-polarized Zak-OTFS and phase-coded waveforms at high SNR, with $\sim 1.5\times$ improvement over FMCW due to no loss in Doppler resolution. Significant improvements with dual-polarized versus unipolarized waveforms.

with equal $h_{HH}^{(p)} = 0.7$ & $h_{HV}^{(p)} = h_{VH}^{(p)} = h_{VV}^{(p)} = 0$, and two targets with unequal $h_{HV}^{(p)} = h_{VH}^{(p)} \in \{0.3, 0.95\}$ & $h_{HH}^{(p)} = h_{VV}^{(p)} = 0$. We observe that polarimetry via FMCW detects false targets in the HH channel and fails to detect the low energy target in the VH channel due to high sidelobes of the waveform. In contrast, polarimetry via phase-coding and Zak-OTFS achieves ideal target detection with minimal sidelobes around the target locations.

B. Target Detection and Parameter Estimation (Quantitative)

We now quantify the performance of target detection and parameter (delay and Doppler) estimation. We consider a single target and model the entries of the 2×2 matrix $\boldsymbol{H}^{(p)}$ as $h_{HH}^{(p)} = a\sigma e^{j\phi}$, $h_{HV}^{(p)} = h_{VH}^{(p)} = a(1-\sigma^2)^{1/2}e^{j\delta}$, and $h_{VV}^{(p)} = b\sigma e^{j\gamma}$, where $a, b \sim$ Bernoulli(0.5) are i.i.d. symmetric Bernoulli random variables, $\sigma \sim U(0,1)$ is a standard uniform random variable, and $\phi, \delta, \gamma \sim U(0, 2\pi)$ are i.i.d. uniform random variables in $[0, 2\pi)$. The delay and Doppler of the target are drawn uniformly at random according to $\tau_t \sim U(0, \tau_p/4)$, $\nu_t \sim U(-\nu_p/8, \nu_p/8)$. We generate 4×10^4 Monte Carlo instances with signal-to-noise ratio (SNR) ranging from -20 to 20 dB.

1) Target Detection: As the detection criteria, we compare the absolute value of the estimated channel at the DD bin corresponding to the target's location (representing the target present hypothesis) with the root-mean-squared value of the channel values at all the locations other than the target's location (representing the target absent hypothesis).

Fig. 3 shows plots of the histograms corresponding to the two hypotheses for all the considered systems. Overlapping histograms indicates poor target detectability. The histograms overlap significantly in the unipolarized systems [Fig. 3(a)–(c)], since a single polarization is insufficient for estimating the full polarimetric scattering response. Polarimetry via FMCW also has significantly overlapping histograms [Fig. 3(d)] due to false detections and high sidelobes of the waveform. Polarimetry via phase-coding and Zak-OTFS has minimal overlap between the histograms [Fig. 3(e) and (f)], indicating their optimality.

Fig. 4(a) shows plots of the receiver operating characteristic (ROC) curve for all the considered systems. Consistent with the findings from Fig. 3, we observe that polarimetry with phase-coded and Zak-OTFS waveforms achieves ideal target detection performance, with performance significantly degrading with FMCW and/or unipolarized transmissions.

2) Parameter Estimation: For parameter estimation, we first detect peaks in the estimated channel following the procedure outlined in [33], which closely mimics the operation of a 2-D constant false alarm rate detector from radar signal processing [21]. We threshold the energy of each channel location by the mean noise

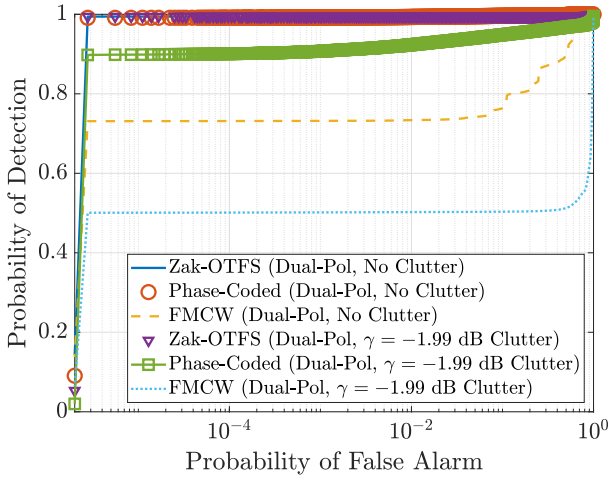

Fig. 5. Instantaneous polarimetry via Zak-OTFS exhibits greater resilience to clutter when compared with competing methods.

energy outside the region of interest ROI $= [-\Delta\tau, \tau_p/4 + \Delta\tau] \times [-\nu_p/8 - \Delta\nu, \nu_p/8 + \Delta\nu]$ ($\Delta\tau$ and $\Delta\nu$ are guard widths to account for spread due to pulse shaping), scaled by an appropriate factor to achieve 10^{-6} false alarm rate [21]. After thresholding, the DD location with the maximum channel energy is the estimated target location.

To fuse the target parameter estimates obtained across multiple polarimetric components, we compute their weighted average using *entropy-based weights*, $w^{(j,i)} = 1 - \mathcal{H}(\widehat{\mathbf{h}}_{\text{eff}}^{(j,i)})/\log_2(MN)$ for all $i, j \in \{V, H\}$, where $\mathcal{H}(\mathbf{h}) = -\sum_{k,l} \left(|\mathbf{h}[k,l]|^2/\sum_{k',l'} |\mathbf{h}[k',l']|^2\right) \log_2 \left(|\mathbf{h}[k,l]|^2/\sum_{k',l'} |\mathbf{h}[k',l']|^2\right)$ denotes the entropy [34] of a DD channel $\mathbf{h}$. Intuitively, such entropy-based weighting prioritizes parameter estimates obtained from polarimetric components with large variation in channel amplitudes (indicating the presence of targets) as opposed to those with little variation in channel amplitudes (indicating noise and the absence of any target). For illustration, consider the extreme case with no targets. Due to mutual unbiasedness, the estimated channel per (14) in this case has a constant energy level of $1/MN$ and an entropy of $\log_2(MN)$, for which the chosen weight is $w^{(j,i)} = 0$, i.e., such components are *not* allowed to bias our estimates.

Fig. 4(b) and (c) shows plots of the root-mean-squared error (RMSE) for delay and Doppler estimation for all the considered systems. The RMSE for delay estimation is similar for polarimetry with FMCW, phase-coding and Zak-OTFS at high SNRs. The Doppler RMSE matches for

polarimetry with phase-coding and Zak-OTFS, with $\sim 1.5\times$ improvement over FMCW, consistent with the explanation in Section II-A. Unipolarized systems have significantly poorer delay and Doppler RMSE. Note that the RMSEs do not improve beyond a certain threshold due to the inherent resolution limits of the chosen waveforms. Future work will design optimal approaches achieving theoretical bounds, e.g., the Cramér–Rao bound [35].

C. Target Detection in Constant-γ Clutter

Fig. 5 shows plots of the detection ROC curve for single-target detection in constant-γ clutter for all dual-polarized systems. For a metropolitan terrain and a carrier frequency of $f_c = 4$ GHz, we obtain the clutter parameter value $\gamma = -1.99$ dB from [36]. Fig. 5 shows that instantaneous polarimetry via Zak-OTFS exhibits greater resilience to clutter when compared with methods based on phase-coded and FMCW transmissions.

V. Conclusion

In this article, we proposed an alternate approach for instantaneous polarimetry using the Zak-OTFS modulation. We designed a spread carrier waveform mutually unbiased to the Zak-OTFS carrier waveform and proposed to simultaneously transmit both waveforms over orthogonal polarizations. Unlike existing methods with computational complexity quadratic in the time–bandwidth product, the proposed method enables instantaneous polarimetry at near-linear complexity and greater clutter resilience. Future work will pursue experimental evaluation and applications to integrated sensing and communication.

References

[1] R. G. Vaughan, "Polarization diversity in mobile communications," *IEEE Trans. Veh. Technol.*, vol. 39, no. 3, pp. 177–186, Mar. 1990.

[2] R. U. Nabar, H. Bolcskei, V. Erceg, D. Gesbert, and A. J. Paulraj, "Performance of multiantenna signaling techniques in the presence of polarization diversity," *IEEE Trans. Signal Process.*, vol. 50, no. 10, pp. 2553–2562, Oct. 2002.

[3] P. Kyritsi, D. C. Cox, R. A. Valenzuela, and P. W. Wolniansky, "Effect of antenna polarization on the capacity of a multiple element system in an indoor environment," *IEEE J. Sel. Areas Commun.*, vol. 20, no. 6, pp. 1227–1239, Aug. 2002.

[4] X. Mao and J. W. Mark, "On polarization diversity in mobile communications," in *Proc. Int. Conf. Commun. Technol.*, 2006, pp. 1–4.

[5] M. R. Andrews, P. P. Mitra, and R. deCarvalho, "Tripling the capacity of wireless communications using electromagnetic polarization," *Nature*, vol. 409, no. 6818, pp. 316–318, Jan. 2001.

[6] T. L. Marzetta, "Fundamental limitations on the capacity of wireless links that use polarimetric antenna arrays," in *Proc. IEEE Int. Symp. Inf. Theory*, Jul. 2002, p. 51.

[7] G. Gupta, B. Hughes, and G. Lazzi, "On the degrees of freedom in linear array systems with tri-polarized antennas," *IEEE Trans. Wireless Commun.*, vol. 7, no. 7, pp. 2458–2462, Jul. 2008.

[8] A. S. Y. Poon and D. N. C. Tse, "Degree-of-freedom gain from using polarimetric antenna elements," *IEEE Trans. Inf. Theory*, vol. 57, no. 9, pp. 5695–5709, Sep. 2011.

[9] W.-M. Boerner and Y. Yamaguchi, "A state-of-the-art review in radar polarimetry and its applications in remote sensing," *IEEE Aerosp. Electron. Syst. Mag.*, vol. 5, no. 6, pp. 3–6, Jun. 1990.

[10] M. Hurtado, J.-J. Xiao, and A. Nehorai, "Target estimation, detection, and tracking," *IEEE Signal Process. Mag.*, vol. 26, no. 1, pp. 42–52, Jan. 2009.

[11] R. Calderbank, S. Howard, and B. Moran, "Waveform diversity in radar signal processing," *IEEE Signal Process. Mag.*, vol. 26, no. 1, pp. 32–41, Jan. 2009.

[12] V. Santalla and Y. M. M. Antar, "A comparison between different polarimetric measurement schemes," *IEEE Trans. Geosci. Remote Sens.*, vol. 40, no. 5, pp. 1007–1017, May 2002.

[13] D. Giuli, L. Facheris, M. Fossi, and A. Rossettini, "Simultaneous scattering matrix measurement through signal coding," in *Proc. IEEE Int. Conf. Radar*, May 1990, pp. 258–262.

[14] S. D. Howard, A. R. Calderbank, and W. Moran, "A simple signal processing architecture for instantaneous radar polarimetry," *IEEE Trans. Inf. Theory*, vol. 53, no. 4, pp. 1282–1289, Apr. 2007.

[15] A. Pezeshki, A. R. Calderbank, W. Moran, and S. D. Howard, "Doppler resilient Golay complementary waveforms," *IEEE Trans. Inf. Theory*, vol. 54, no. 9, pp. 4254–4266, Sep. 2008.

[16] A. R. Calderbank, S. D. Howard, W. Moran, A. Pezeshki, and M. Zoltowski, "Instantaneous radar polarimetry with multiple dually-polarized antennas," in *Proc. 40th Asilomar Conf. Signals, Syst. Comput.*, 2006, pp. 757–761.

[17] B. Hochwald and A. Nehorai, "Polarimetric modeling and parameter estimation with applications to remote sensing," *IEEE Trans. Signal Process.*, vol. 43, no. 8, pp. 1923–1935, Aug. 1995.

[18] C. Lopez-Martinez, E. Pottier, and S. R. Cloude, "Statistical assessment of eigenvector-based target decomposition theorems in radar polarimetry," *IEEE Trans. Geosci. Remote Sens.*, vol. 43, no. 9, pp. 2058–2074, Sep. 2005.

[19] M. Jankiraman, *FMCW Radar Design*. Norwood, MA, USA: Artech House, 2018.

[20] F. Uysal, "Phase-coded FMCW automotive radar: System design and interference mitigation," *IEEE Trans. Veh. Technol.*, vol. 69, no. 1, pp. 270–281, Jan. 2020.

[21] M. I. Skolnik, *Introduction to Radar Systems*, vol. 3. New York, NY, USA: McGraw-Hill, 1980.

[22] N. Levanon and E. Mozeson, *Radar Signals*. Hoboken, NJ, USA: Wiley, 2004.

[23] A. Harms, W. U. Bajwa, and R. Calderbank, "Identification of linear time-varying systems through waveform diversity," *IEEE Trans. Signal Process.*, vol. 63, no. 8, pp. 2070–2084, Apr. 2015.

[24] D. Nisar, S. Khan Mohammed, R. Hadani, A. Chockalingam, and R. Calderbank, "Zak-OTFS for identification of linear time-varying systems," 2025, *arXiv:2503.18900*.

[25] N. Mehrotra, S. Rao Mattu, S. Khan Mohammed, R. Hadani, and R. Calderbank, "Discrete radar based on modulo arithmetic," 2025, *arXiv:2508.15671*.

[26] J. Schwinger, "Unitary operator bases," *Proc. Nat. Acad. Sci. USA*, vol. 46, no. 4, pp. 570–579, Apr. 1960.

[27] J. Bai, G. Wei, J. Shao, X. Wang, and Z. Fei, "Design of orthogonal polyphase code set based on multipulse joint processing," *IEEE Trans. Aerosp. Electron. Syst.*, vol. 60, no. 6, pp. 8901–8913, Dec. 2024.

[28] S. K. Mohammed, R. Hadani, and A. Chockalingam, *OTFS Modulation: Theory and Applications*. Hoboken, NJ, USA: Wiley, 2024.

[29] S. K. Mohammed, R. Hadani, A. Chockalingam, and R. Calderbank, "OTFS—A mathematical foundation for communication and radar sensing in the delay-Doppler domain," *IEEE BITS Inf. Theory Mag.*, vol. 2, no. 2, pp. 36–55, Nov. 2022.

[30] S. K. Mohammed, R. Hadani, A. Chockalingam, and R. Calderbank, "OTFS—Predictability in the delay-Doppler domain and its value to communication and radar sensing," *IEEE BITS Inf. Theory Mag.*, vol. 3, no. 2, pp. 7–31, Jun. 2023.

[31] N. Mehrotra, S. R. Mattu, and R. Calderbank, "Zak-OTFS with spread carrier waveforms," *IEEE Wireless Commun. Lett.*, vol. 14, no. 10, pp. 3244–3248, Oct. 2025.

[32] C. Parisi, V. Khammammetti, R. Calderbank, and L. Huie, "Over-the-air transmission of zak-OTFS with spread pilots on sub-THz communications testbed," 2025, *arXiv:2504.15947*.

[33] M. Ubadah, S. Khan Mohammed, R. Hadani, S. Kons, A. Chockalingam, and R. Calderbank, "Zak-OTFS to integrate sensing the I/O relation and data communication," 2024, *arXiv:2404.04182*.

[34] T. Zeng, R. Wang, and F. Li, "SAR image autofocus utilizing minimum-entropy criterion," *IEEE Geosci. Remote Sens. Lett.*, vol. 10, no. 6, pp. 1552–1556, Nov. 2013.

[35] H. L. Van Trees, *Detection, Estimation, and Modulation Theory, Part III: Radar-Sonar Signal Processing and Gaussian Signals in Noise*. Hoboken, NJ, USA: Wiley, 2001.

[36] M. W. Long, *Radar Reflectivity of Land and Sea*, 1975.

Nishant Mehrotra received the B.Tech. degree (Hons.) in electronics and electrical communication engineering from the Indian Institute of Technology, Kharagpur, India, in 2018, and the M.S. and Ph.D. degrees in electrical and computer engineering from Rice University, Houston, TX, USA, in 2020 and 2024, respectively.

He is currently a Postdoctoral Associate at Duke University, Durham, NC, USA. His research interests include radar sensing, next-generation wireless systems, joint sensing-communication, and information theory.

Sandesh Rao Mattu received the B.Tech. degree in electronics and communication engineering from Manipal Institute of Technology, Manipal, India, in 2016, and the Ph.D. degree from the Department of Electrical Communication Engineering, Indian Institute of Science, Bengaluru, India, in 2024.

From 2016 to 2018, he was with Philips, Bengaluru. He worked for Samsung Research, Bengaluru, from January 2024 to August 2024. He is currently a Postdoctoral Associate at Duke University, Durham, NC, USA. His research interests include channel estimation, wireless communications, and applications of deep learning in communication.

Robert Calderbank (Life Fellow, IEEE) received the B.Sc. degree in mathematics from Warwick University, Coventry, U.K., in 1975, the M.Sc. degree in mathematics from Oxford University, Oxford, U.K., in 1976, and the Ph.D. degree in mathematics from California Institute of Technology, Pasadena, CA, USA, in 1980.

He is a Distinguished Professor of Electrical and Computer Engineering, Computer Science and Mathematics, Duke University. He started his career in the Mathematical Sciences Research Center at Bell Labs, and he left AT&T in 2003 as the Vice President for Research. He directed the Program in Applied and Computational Mathematics, Princeton University, before joining Duke University in 2010.

Dr. Calderbank received the 2015 Hamming Medal, and the 2015 Shannon Award. He is known for contributions to voiceband modem technology at the dawn of the Internet, and for contributions to wireless communication that are incorporated in billions of cell phones. He has also made contributions to quantum error correction that provide the foundation for fault tolerant quantum computation. He was elected to the National Academy of Engineering in 2005, to the National Academy of Inventors in 2015, and to the American Academy of Arts and Sciences in 2023.